NREL
NATIONAL RENEWABLE ENERGY LABORATORY

NREL Gearbox Reliability Collaborative: Comparing In-Field Gearbox Response to Different Dynamometer Test Conditions

Preprint

William LaCava, Jeroen van Dam, and Robb Wallen
National Renewable Energy Laboratory

Brian McNiff
McNiff Light Industry

Presented at WINDPOWER 2011
Anaheim, California
May 23-25, 2011

NREL is a national laboratory of the U.S. Department of Energy, Office of Energy Efficiency & Renewable Energy, operated by the Alliance for Sustainable Energy, LLC.

Conference Paper
NREL/CP-5000-51690
August 2011

Contract No. DE-AC36-08GO28308

NOTICE

Available electronically at http://www.osti.gov/bridge

Available for a processing fee to U.S. Department of Energy
and its contractors, in paper, from:

U.S. Department of Energy
Office of Scientific and Technical Information

P.O. Box 62
Oak Ridge, TN 37831-0062
phone: 865.576.8401
fax: 865.576.5728
email: mailto:reports@adonis.osti.gov

Available for sale to the public, in paper, from:

U.S. Department of Commerce
National Technical Information Service
5285 Port Royal Road
Springfield, VA 22161
phone: 800.553.6847
fax: 703.605.6900
email: orders@ntis.fedworld.gov
online ordering: http://www.ntis.gov/help/ordermethods.aspx

Cover Photos: (left to right) PIX 16416, PIX 17423, PIX 16560, PIX 17613, PIX 17436, PIX 17721

Printed on paper containing at least 50% wastepaper, including 10% post consumer waste.

Table of Contents

List of Figures

List of Abbreviations

DOE	Department of Energy
NREL	National Renewable Energy Laboratory
TDC	Top Dead Center
NTL	Non-Torque Load
FFT	Fast Fourier Transform
GRC	Gearbox Reliability Collaborative
IEC	International Electrotechnical Commission
LDD	Load Data Distribution
LSS	Low Speed Shaft (Main Shaft)
HSS	High Speed Shaft
CRB	Cylindrical Roller Bearing
VFD	Variable Frequency Drive
Dyno	Dynamometer
UW	Upwind
DW	Downwind
Np	N repetitions per revolution of the main shaft
V_{in}	Cut-in wind speed
V_{rated}	Maximum rated wind speed

1 Summary

The NREL/ DOE Gearbox Reliability Collaborative has been reviewing the design process of wind turbine gearboxes in order to identify ways to improve the reliability of this fundamental component. As part of this effort, two 750-kilowatt (kW) gearboxes were removed from an operating population and redesigned and rebuilt to meet current megawatt (MW) power standards using state-of-the-art technology. To date, 300+ hours of operational data, including over 125 signals, have been collected in the field and from NREL dynamometer testing on a 750-kW wind turbine platform. This data includes both internal and external loads, motions, deflections and other response during a broad range of operating modes and conditions.

This paper compares measured gearbox response in the NREL dynamometer to gearbox response during field testing. It then describes the way in which dynamometer testing has been improved to better represent field loading conditions. Conclusions and recommendations are made for augmented dynamometer testing.

2 Background

The National Renewable Energy Laboratory (NREL), a U.S. Department of Energy laboratory, has undertaken the difficult task of identifying the gaps and sensitivities in the design process that may contribute to the premature failure of wind turbine gearboxes. To this end, NREL has brought together the different parties involved in the wind turbine and component design, manufacture and operation through a program called the Gearbox Reliability Collaborative (GRC) that has been described previously (1,2). The GRC has utilized a comprehensive approach to reviewing the complete drivetrain design process using current design tools and validating them with operational test data.

There are four main GRC research activities:

- testing with full-scale dynamometer and in the field
- building a database of observed failures
- performing drivetrain design, analysis and modeling
- investigating how condition monitoring can improve reliability.

This paper discusses selected parts of the testing and data analysis activities.

The testing utilized two identical, highly instrumented 750-kW gearboxes with over 125 signals each. The gearboxes were removed from the field and rebuilt to current state-of-the-art-design including active lubrication, different bearing configurations, modified gear micro-geometry, and a floating sun for improved load distribution. Measurements included bearing and gear load distributions, internal and external motions, deflections and accelerations, and temperatures.

Currently, hundreds of hours of experimental data have been obtained from testing the two gearboxes in the NREL 2.5-MW dynamometer facility and on a field test turbine. This data provides important information for comparing the behavior of the gearbox components in normal wind turbine operating modes with the behavior in dynamometer testing.

Historically, most dynamometer testing has been with steady state applied torque and limited (static) non-torque loading. Yet during field operation, wind turbine gearboxes are subject to continuously fluctuating loads caused by variations in the wind and control actions. These conditions must be considered in the design process (6) but are difficult to validate in a dynamometer. The GRC is working to improve the capability of the NREL dynamometer (and dynamometer testing in general) to more accurately reproduce in-field operation and response.

Additionally, the GRC data is being used to help improve analytical tools through the partnerships formed in the project. A wind turbine gearbox is comprised of many hundreds of moving and stationary parts interacting in a complex dynamic environment. Modeling this complex system efficiently and verifying that all the parts work together as designed has proven to be difficult (3). This is evidenced by problems occurring in the field with many gearbox designs (4,5). High confidence design verification through analysis and in a dynamometer could be critical in identifying potential problems in this key component at the pre-production prototype stage.

This paper describes the pertinent parts of the GRC field and dynamometer test programs and compares the measured gearbox response in the NREL dynamometer to operation in the field. The field test provided real wind turbine data which could be replicated in the dynamometer for controlled testing. Results are presented from the initial attempts to apply time history-based loads from the field to the gearbox in the dynamometer.

3 GRC Test Program Description

3.1 Overall Test Program

The main objective of the GRC tests was to build an understanding of how normal wind turbine loading conditions and transient events translate into gear and bearing response, including reactions, load distribution, displacements, temperature, stress, and slip. This information will help improve bearing selection and integration, gear and bearing design and provide input to relevant design and application standards (6,7,8). In the process, the acquired test data will be used to validate wind turbine drivetrain, gear, and bearing analytical tools, as well as assess a comprehensive matrix of design loads required for proper wind turbine gearbox design.

The wind turbine drivetrain design is shown in Figure 1. The gearboxes feature a standard arrangement of first stage planetary and two parallel stages on a 3 point support (main bearing and elastomeric trunion supports). Both units were identically instrumented to allow for a broad array of measurements to meet the objectives. One of the gearboxes was tested in the NREL 2.5-MW

Dynamometer Test Facility, and the other was installed and operated on an upwind, stall-controlled, 3 bladed turbine at the Xcel Energy Ponnequin wind plant.

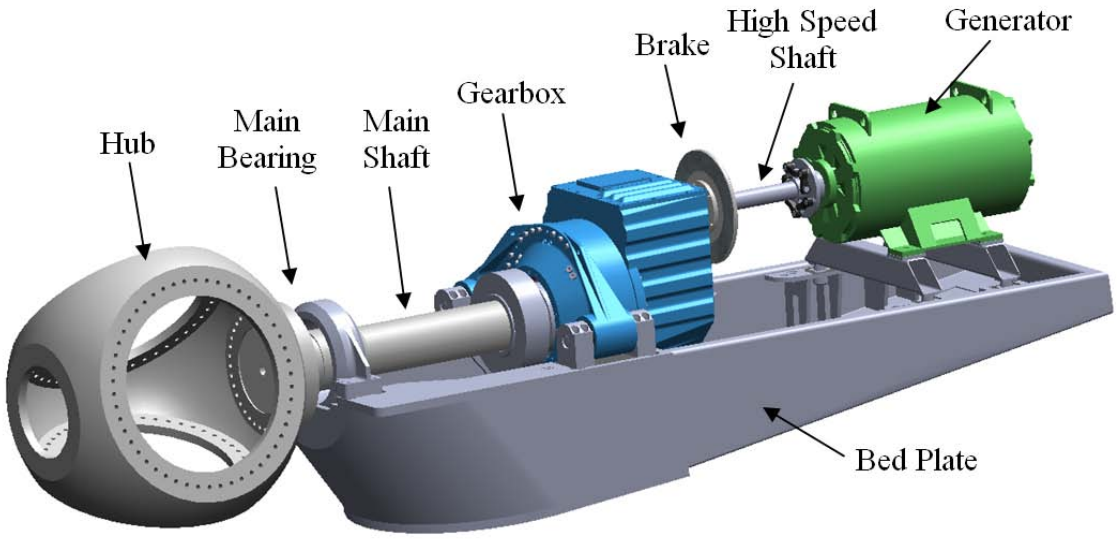

Figure 1. GRC drivetrain.

Achieving the test objectives was highly dependent on making measurements that correctly characterized the behavior of the critical drivetrain elements under the various loading scenarios. The original measurement goals are listed as follows:

- Relative displacement of planet carrier rim to gear housing
- LSS axial motion displacement relative to gear housing
- Planet load share and annulus gear face width load distribution
- Main shaft azimuth angle to sync with annulus gear stain gauges
- Planet bearing radial load distribution
- HSS axial displacement relative to gear housing
- HSS locating bearing axial load distribution
- Planet gear motion relative to carrier
- Sun pinion radial & axial motion
- Relative motion of gearbox to base frame
- Relative motion of LSS relative to base frame
- Relative motion of HSS relative to generator
- Planet bearing slip

A more complete description of the testing is included in a forthcoming NREL publication (9).

3.2 Field Testing

The field test was used to characterize motions and responses of the drivetrain elements during normal and unique loading situations. These include transient accelerations and decelerations due to rapid increase in wind speed at start-up or control actions such as shifting between generators and shutdown.

There were additional signals installed on the field test intended to:

- validate load assumptions for the analysis team to tune the aeroelastic models and modify the dynamic and multibody analysis codes
- provide means to verify that testing in the dynamometer can accurately reproduce in-field response
- provide direct connection between internal gearbox responses to commonly measured and simulated environmental conditions, primary rotor forces and moments and typical control situations.

The field test matrix is shown in Table 1 provides a summary of the number of events recorded in the field test program.

Table 1. Field Test Matrix – Events or Time

	Wind Conditions		
Situation	**V_{in}**	**$V_{in}<V<V_{rated}$**	**$>V_{rated}$**
Start up	2	2	2
brake stop	2	2	2
E-stop	2	2	2
Gen shift down	2	2	2
Gen shift up	2	2	2
Accelerations > 1 rpm/sec	2	2	2
Normal operation	3 x 10 min	3 x 10 min	3 x 10 min
Off yaw operation	3 x 10 min	3 x 10 min	3 x 10 min
Parked	3 x 10 min	3 x 10 min	3 x 10 min

Over 300 hours of data was collected in a broad range of wind speeds and torque levels. Figure 2 and Figure 3 show the collection statistics taken in 10 minute averages. The field test collected wind speed conditions up to 26 m/s and torque transients from 735 kNm (200% of rated torque) to -273 kNm. The range of measurement values allowed for an appropriate selection of dynamometer loading conditions that formed the Phase 2 test program.

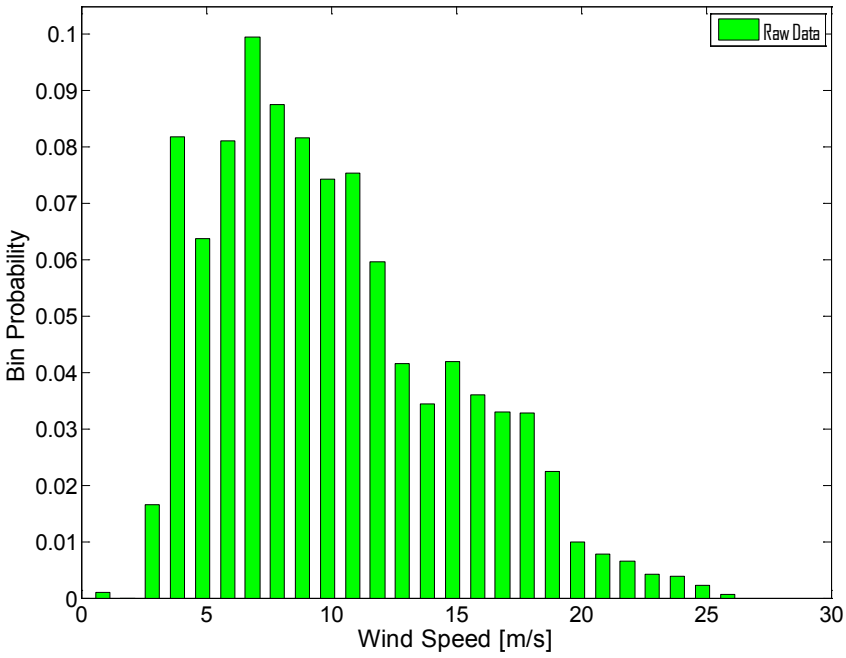

Figure 2. Wind speed histogram - field test data.

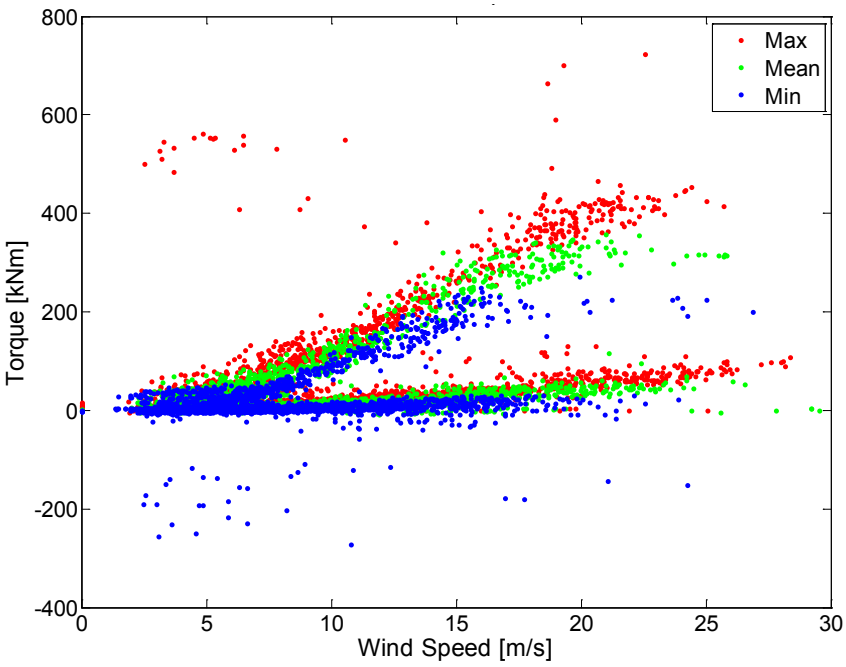

Figure 3. LSS torque vs. wind speed - field test data.

3.3 Dynamometer Testing

The dynamometer test was configured to match, as closely as possible, the response and situations measured in the field. To accomplish this, a complete turbine main frame was installed in the dynamometer facility.

The 1st phase of dynamometer testing involved run-in, signal checks and static load response and is described in the NREL test plan (9). In Phase 2 of dynamometer testing, a rig was constructed to apply non-torque forces and moments to the test article (see Figure 4). This system could apply dynamic non-torque loading in order to help evaluate the effect on internal gearbox response.

One of the objectives of the Phase 2 dynamometer test was to investigate the effects of increased complexity of loading (static and dynamic non-torque loading, torque feedback control, etc) to more accurately reproduce in-field response. This included developing a repeatable sequence of drivetrain speed and load changes to facilitate the comparison of test setup configuration changes.

Figure 4. NREL/PIX18952: Non-torque load mechanism in NREL dynamometer.

The basic test matrix for the Phase 2 dynamometer testing is shown in Table 2. The load cases selected increase in complexity from steady torque to in-field, data driven dynamics. The progressive approach of the test plan provided good insight on the loading conditions that generate uncharacteristic gearbox behavior that would not be observed in typical dynamometer testing.

Table 2. General Test Matrix for Phase 2 Dynamometer Tests

	Load case	Objective
1	Steady torque	Baseline dynamometer testing
2	Steady NTL and steady torque	Testing to account for rotor overhang moment
3	Dynamic torque without NTL	Tuning of torque control loop at several frequencies
4	Dynamic torque with steady NTL	Identify effect of NTL on torque control loop
5	Steady torque with dynamic NTL	Tune NTL system, compensation for any 1P effects
6	Dynamic torque and dynamic NTL	Simple case to prove concept
7	Simulation of field data with dynamic torque and NTL	Demonstrate difference in dynamometer loading and field loading

3.4 Measurement Setup

Torque and two orthogonal bending moments (see Figure 5) were measured on the main shaft between the main bearing and the gearbox using strain gauges in full bridge arrangements.

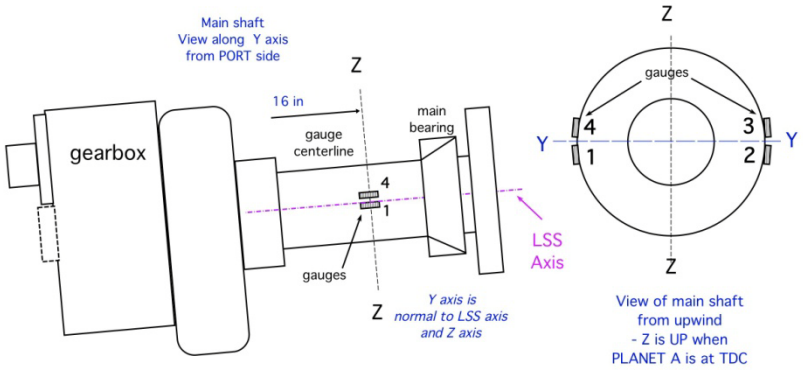

Figure 5. Main shaft gauges - example.

For the planet bearings, strain gauges were applied to 3 axial slots machined into the inner surface of the inner ring of all 6 planet CRB bearings as shown on the left graphic in Figure 6. The slots were located at different locations in the bearing load zone for each planet, but they all had slots at the orthogonal to the sun-planet axis (referred to here as TDC). Two gauge sets in each slot and two bearings on each planet provided an axial distribution of radial loads at 4 locations along each planet pin (right graphic in Figure 6). These gauges were calibrated to loads applied to the fully assembled planet pins and bearing pairs in a bench-top test setup (10).

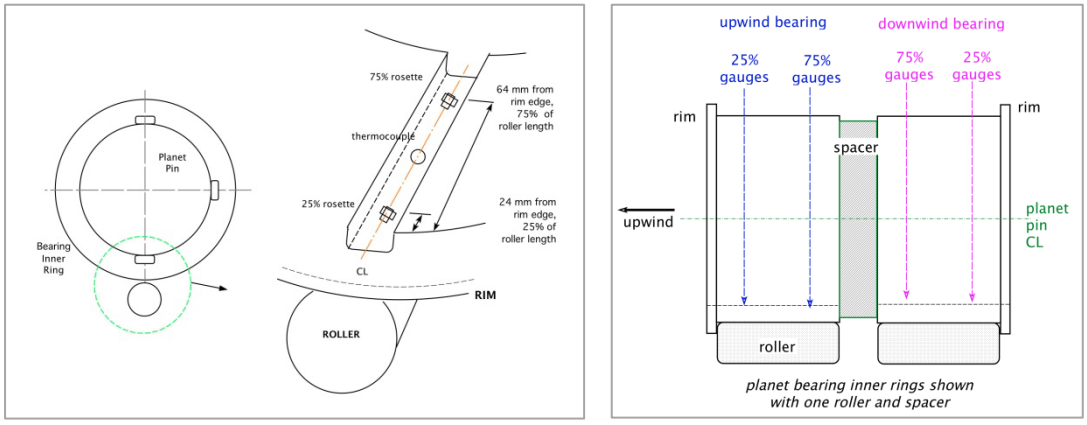

Figure 6. Gauges in machined slots in planet bearing inner rings.

Ring gear load distribution was measured using a cascade of strain gauges placed in the tooth roots at 8 axial locations (oriented circumferentially), as shown in Figure 7. Three tooth load distributions at 0°, 120°, and 240° were measured for each rotation of the low speed shaft from a total of 24 strain gauges. The planets were labeled A, B, and C in counterclockwise fashion with Planet A at TDC when the main shaft azimuth angle equaled 0 degrees.

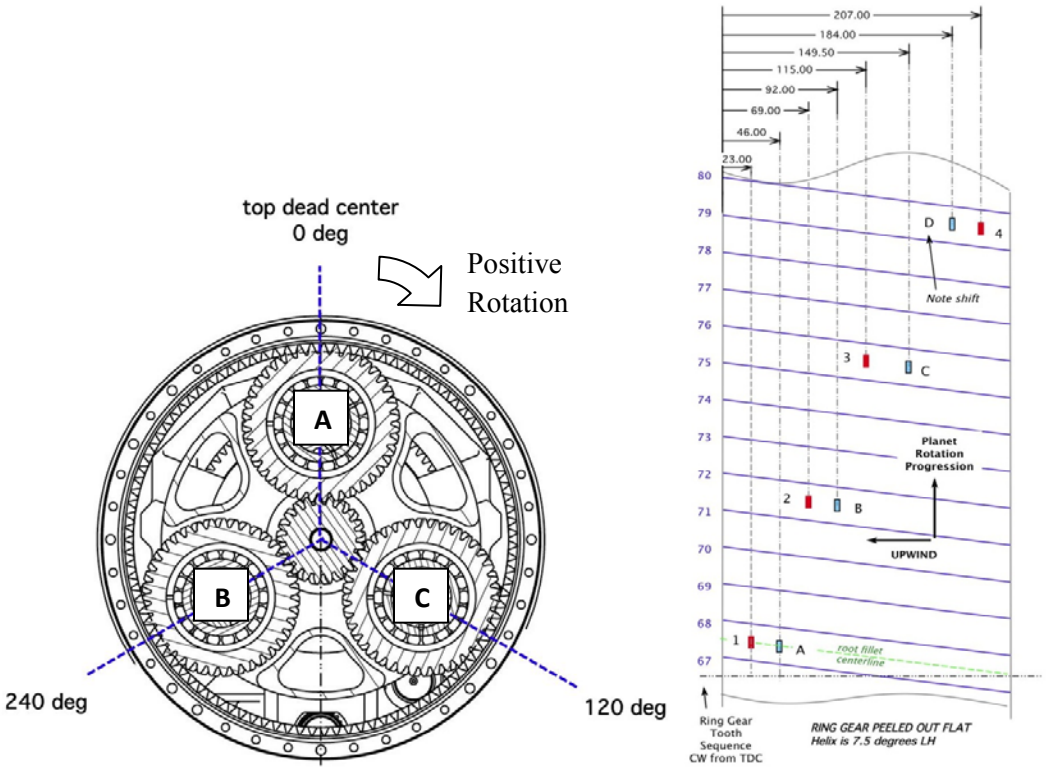

Figure 7. Ring gear load distribution measurement.

4 Data Analysis and Processing

4.1 Comparison of Field and Dynamometer Gearbox Response

In this clause, gearbox measurements taken while running at 100% load in the field are compared to a 100% steady state load case tested in the dynamometer. Signals are compared in the time and frequency domains. Additional static dynamometer test cases are identified and used for comparison to field variations where indicated.

Main Shaft Torque

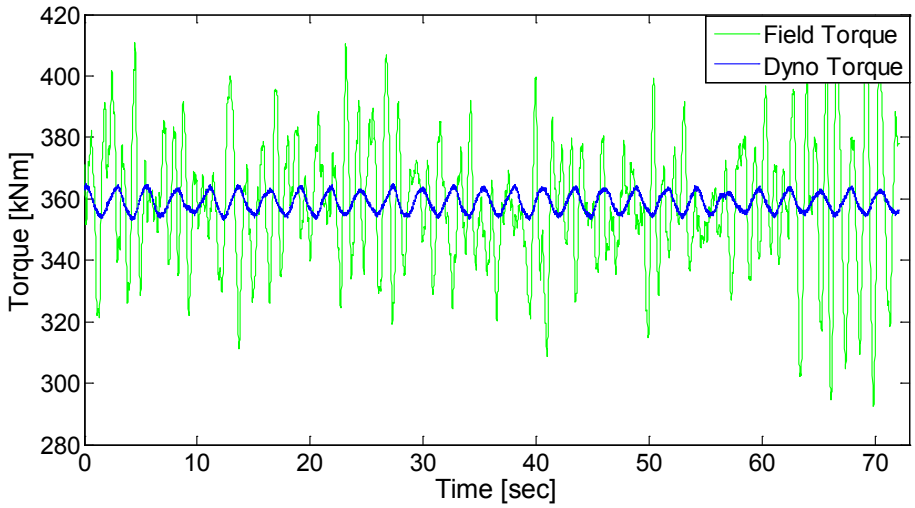

Figure 8. Variations in LSS torque in field and dynamometer tests

The gearbox main shaft torque response in dynamometer testing matches the average magnitude of the shaft torque in field testing, but there is much less torque variance in the dynamometer (see Figure 8). The constant torque applied in the dynamometer excites the shaft at its rotation frequency alone (see Figure 8), while the dominating excitation frequency in the field is 3p, corresponding to the blade pass frequency. The field torque also shows energy at the drivetrain natural frequency and multiples of the blade pass frequency.This is a significant gearbox loading difference not captured with a standard time at level dynamometer test.

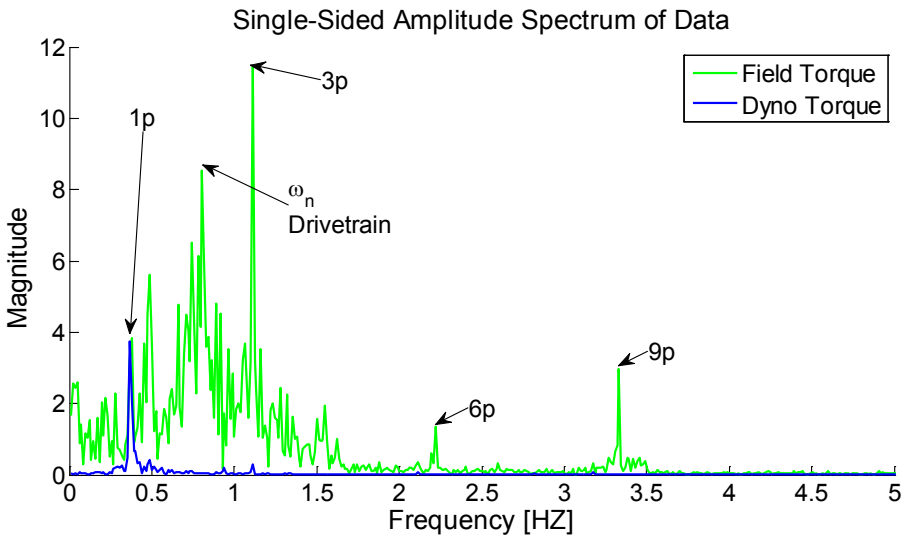

Figure 9. FFT of LSS torque in field and dyno tests.

Main Shaft Bending

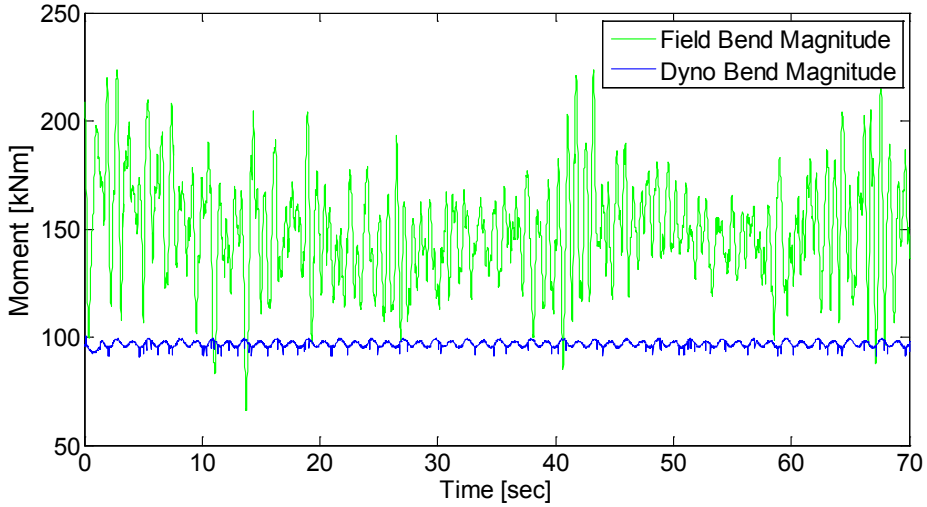

Figure 10. Field and dyno test shaft bending vs rotor azimuth.

Figure 10 shows the measured shaft bending magnitude for field and dynamometer test cases. The gearbox in this 3-point drivetrain support is not completely uncoupled from the rotor moments and forces. The main shaft experiences a larger amount of static bending in the field since the overhung weight of the rotor is larger than the combined weight of the dynamometer jack shaft, the couplings and the non-torque loading equipment. Wind variation in the field imparts shifting asymmetric rotor loads as well, and these greatly affect the shaft bending.

An FFT of the stationary Y and Z components of main shaft bending is shown in Figure 11. It can be seen that the main shaft experiences significantly higher bending variation in the field than it is

subjected to in standard, torque-only dynamometer testing for the reasons mentioned above. The coordinate system used in this document is shown in Appendix A.

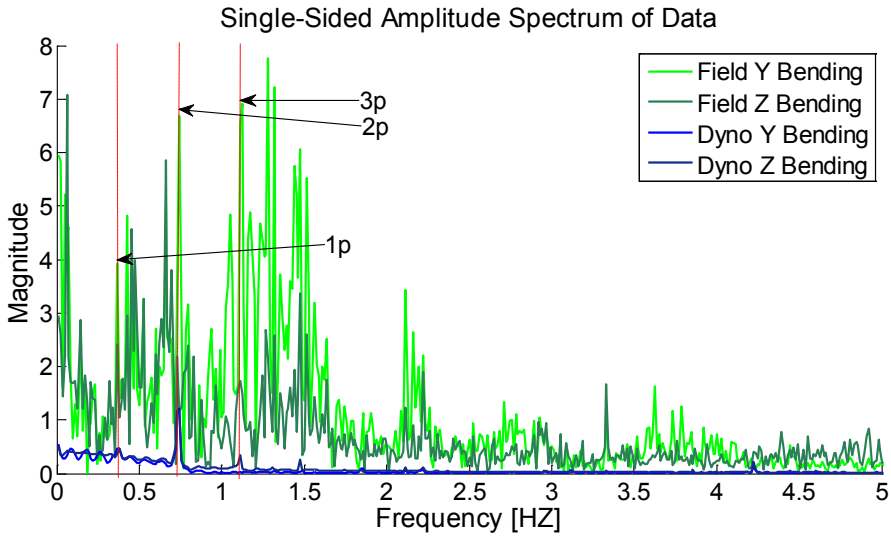

Figure 11. FFT of Y and Z components of shaft bending in field and dyno testing.

In order to examine the importance of variations in main shaft bending on the gearbox response, seven distinct magnitudes of vertical non-torque loads were applied in the dynamometer while operating at 100% power. The ring gear load distribution was then evaluated as a function of the resultant main shaft bending moment.

Figure 12 shows the change in ring gear load distribution caused by the bending condition in the main shaft. As the Y direction main shaft moment increases, upwind edge loading of the ring gear teeth at the 120° location increases. Conversely, downwind edge loading increases at the 240° degree location. At both ring gear locations, the increased edge loading at one end of the teeth is coupled with a decrease of the load at the other edge.

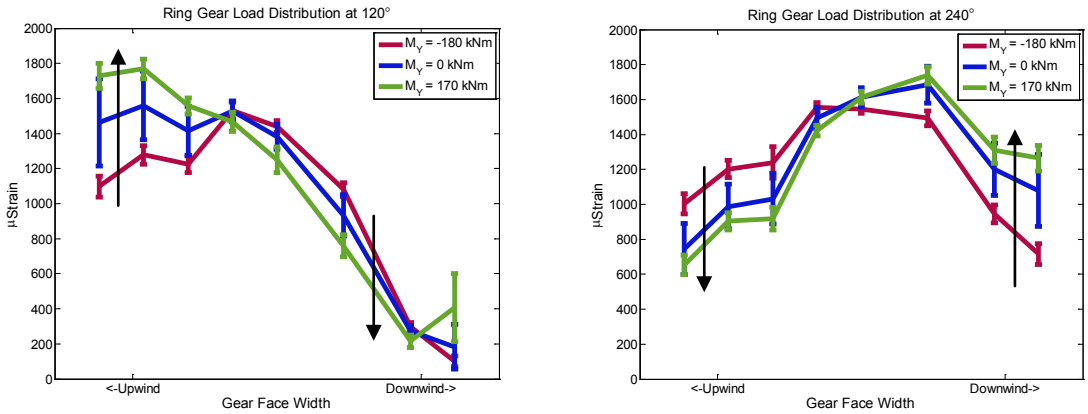

Figure 12. Effect of applied shaft moment on ring gear load distribution.

In order to quantify this edge loading effect, a third order polynomial was fit to the strain distributions and the centroid of the area under each load distribution curve is calculated using the formula:

$$Centroid = \frac{\int x \cdot \varepsilon(x) dx}{\int \varepsilon(x) dx}$$

Equation 1

where x is the fraction of gear face width (0 to1), and $\varepsilon(x)$ is the strain value at that location. By plotting these centroid values versus main shaft bending, a strong correlation is observed between main shaft Y bending moment and the load centroid on the ring gear at 120° and 240°, as shown in Figure 13.

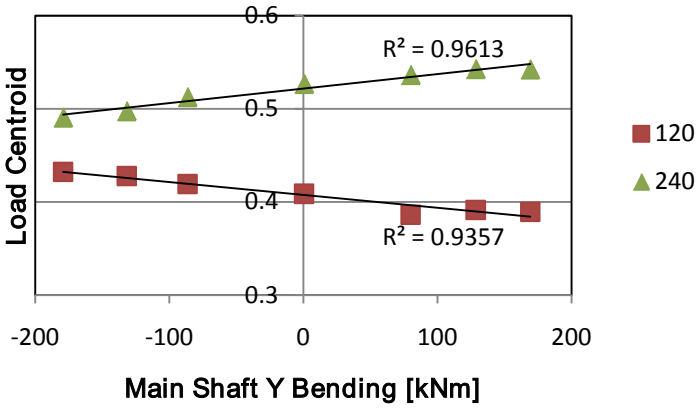

Figure 13. Load centroid sensitivity to Y bending.

Ring gear tooth load misalignment of this type has been shown to have an adverse effect on gearbox life (11). Gear tooth edge loading or poor load distribution is a deterrent to gear life that is

generally controlled by micro geometry and crowning of the gear tooth. These corrections can compensate for small deflections and misalignments of the gearing system. However the introduction of the bending loads as shown above can potentially undermine the microgemoetry and result in undesired loading condition for the gears. Further testing and understanding of the effects of the bending loads is necessary, however the potential negative effects of non-torque loading is evident.

Planet Bearing Strains

The planet bearing strain signals show generally good agreement in magnitude for the field and dynamometer test cases with the exception of planet C, as shown in 3 of the signals presented in Figure 14. By processing the signals into peak-valley ranges and calculating the FFT, a 3p magnitude change can be observed in the field data which does not occur in dynamometer testing, as shown in Figure 15. However, the main modulation is once per revolution for both cases, and is shown in shorter period time series of a raw bearing signal in Figure 16.

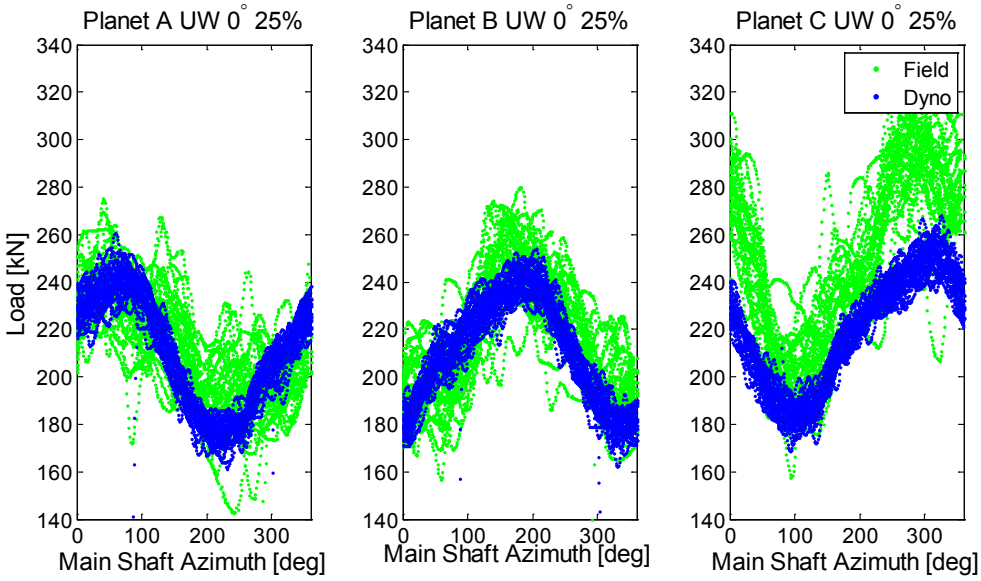

Figure 14. Similar planet bearing load magnitudes (at TDC).

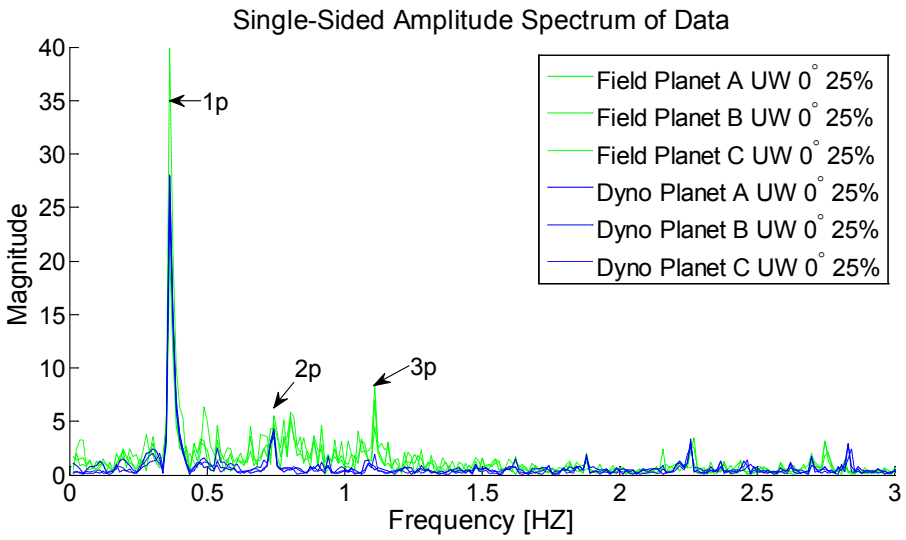

Figure 15. FFT of peak-valley strain magnitudes.

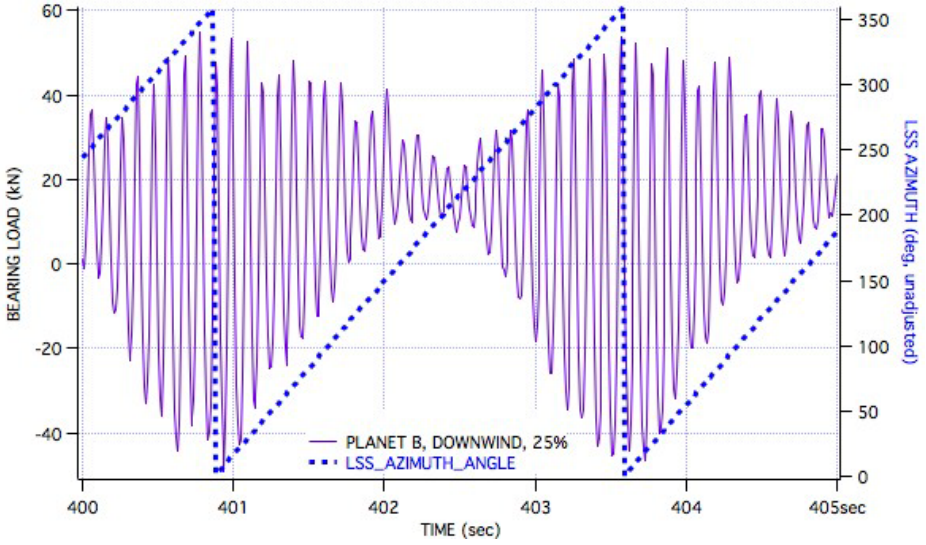

Figure 16. Bearing strain signal modulation with LSS/carrier rotation.

The load share of the planets can be calculated for each time step using these bearing inner ring radial load measurements taken at four axial locations in the TDC slot on each planet along the pins (see Figure 17). The mesh load factor Kγ (12, 13) is calculated for each planet, *i,* using the equation

$$K\gamma_i = \frac{\int \varepsilon_i(x)dx}{\frac{1}{3}\sum_{i=1}^{3}\int \varepsilon_i(x)dx}$$

Equation 2.

The Kγ results for the field data are plotted versus the rotation of the main shaft and carrier in Figure 17. A value of 1 would indicate that all 3 planets are equally loaded. The time varying planet load share is related to planet/sun gear misalignment, and this has been reproduced in modeling by Crowther et al (11). Planet load share in this sense is not heavily influenced by dynamic loading above 1p.

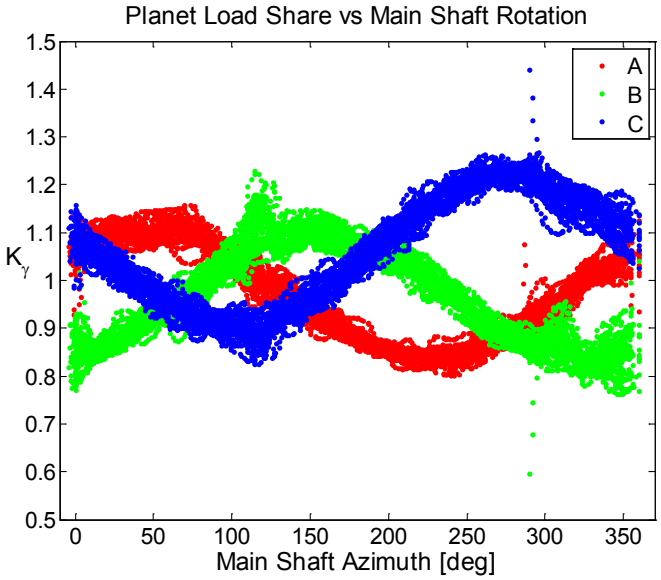

Figure 17. Planet load share derived from bearing loads.

The dynamic loading conditions experienced in the field may influence planet bearing load zones, which experience a dynamic upwind/downwind shift. The helical planet-ring and planet-sun gear mesh create a force couple on the planet gear about the axis tangent to the path of its center of gravity. This helical moment induces a shift in the upwind and downwind bearing load zones, as shown in the bearing load zone schematic of Figure 18(left side). These opposing load zone shifts are observed in the strain measurements for planet A upwind and downwind bearings in the field (Figure 18, right side).

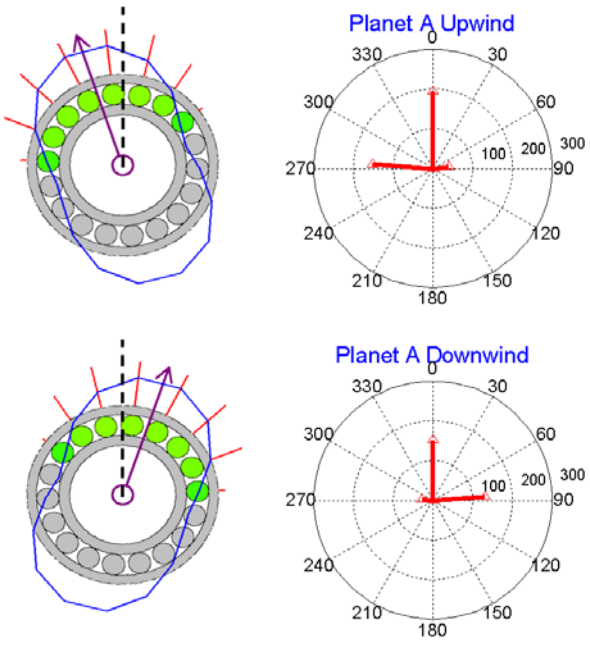

Figure 18. Planet A bearing loading vectors (at gauges).

These upwind and downwind bearing load zone shifts, the axial shuttling forces caused by varying centroid of the gear mesh forces, and friction forces caused by gear sliding operate at higher frequencies than 1p. These behaviors must be studied more in depth to determine whether higher order torque and bending loads have a significant effect.

4.2 Simulating Field Loading Conditions in the Dynamometer

Dynamic Torque Control

An attempt to reproduce a main shaft torque time history from the field was conducted. In the existing 2.5-MW dynamometer, the control problem proved challenging due to system properties. Firstly, the coupled response of the test article and dynamometer exhibited torsional resonances within the frequency band of interest. Secondly, the current source VFD driving the dynamometer responds slowly to torque command changes, resulting in poor system response and closed loop instability in the operating band. The solution was to apply offline, open loop control techniques to achieve the best response.

The system was first run with band limited pseudo-random noise in order to obtain the transfer function. The input command was then compensated with a calculated error (the difference between command torque and output torque) and iterated upon to minimize the error.

A comparison of the field and dynamometer torque measurements is shown in Figure 19. As can be seen in Figure 20, the system resonances introduced extra torque dynamics into the testing. The

response was hampered by the slow dynamometer response, but the concept was successfully demonstrated nontheless. The lessons learned are being applied to the new 5 MW dynamometer to be constructed at NREL in the very near future.

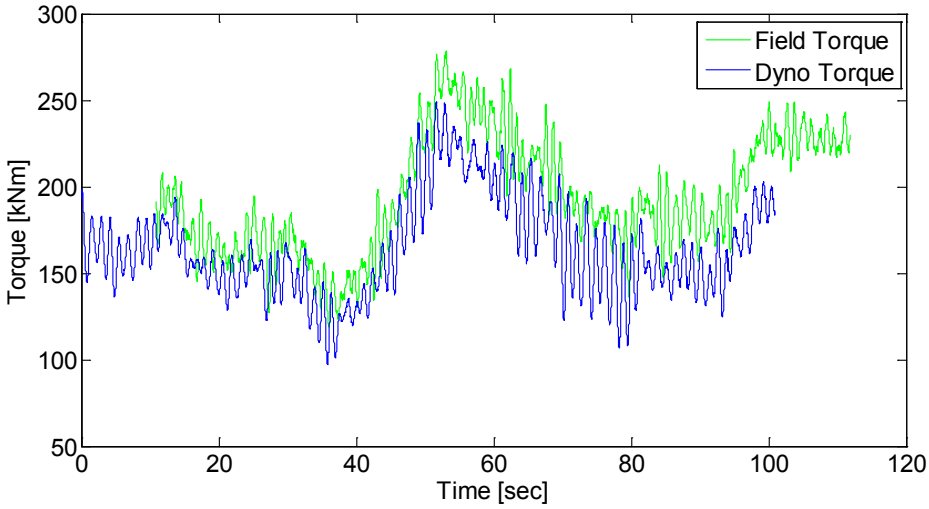

Figure 19. Time series of field torque data reproduced in dynamometer testing.

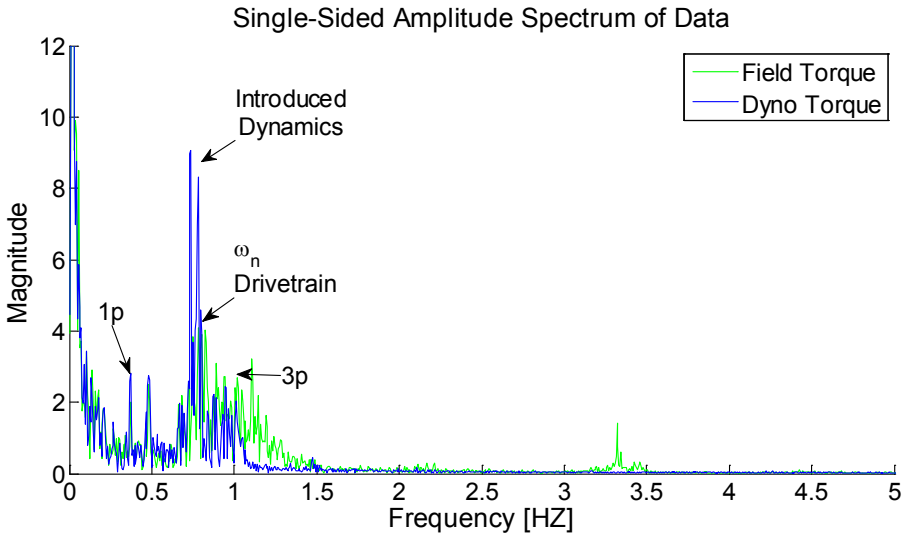

Figure 20. FFT of field torque data reproduced in dynamometer testing.

Dynamic Non-Torque Loading Control

Non-torque loads were applied in the dynamometer using three closed loop servo-hydraulic actuators with displacement and force feedback. The control software translated magnitude and direction commands loaded from a time history file into separate actuator forces. The force control loops are closed separately for the two actuators. All commands were generated at 100 Hz in open

loop without feedback from the main shaft bending measurements. The control block diagram is shown in Figure 21.

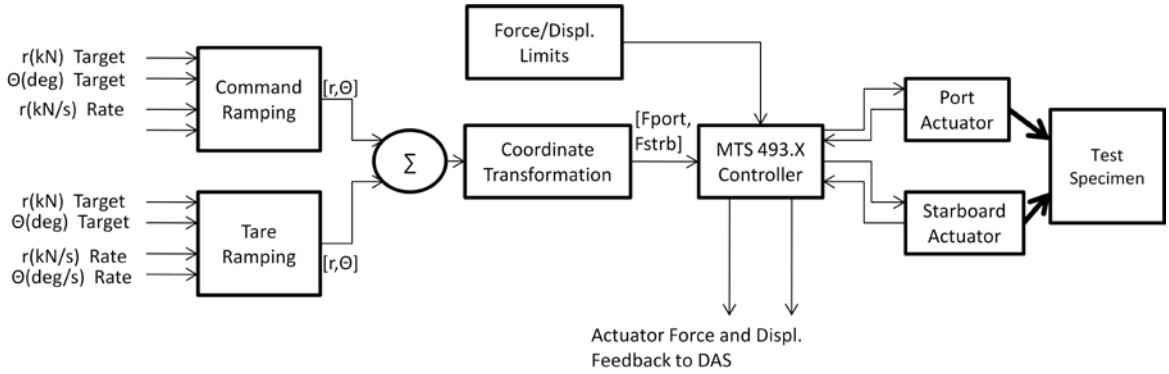

Figure 21. Dynamic NTL control diagram.

Main shaft bending magnitude and direction data from the field testing were fed into the NTL system to demonstrate the concept. The data was low pass filtered to 2 Hz and a comparison of main shaft bending magnitude for the field and dynamometer cases is shown in Figure 22. The system calibration contributed to the magnitude error. The time varying 3p excitation was reproduced successfully as seen in Figure 23.

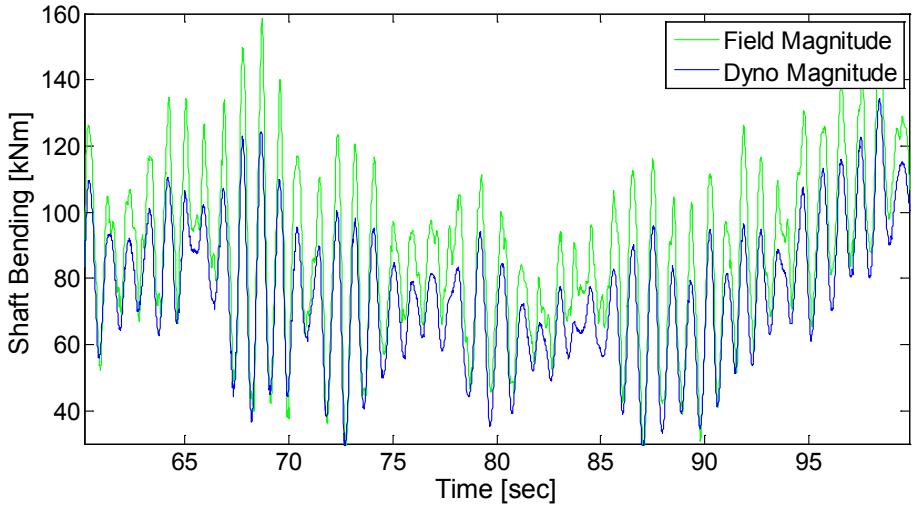

Figure 22. Time series of field shaft bending reproduced in dynamometer testing.

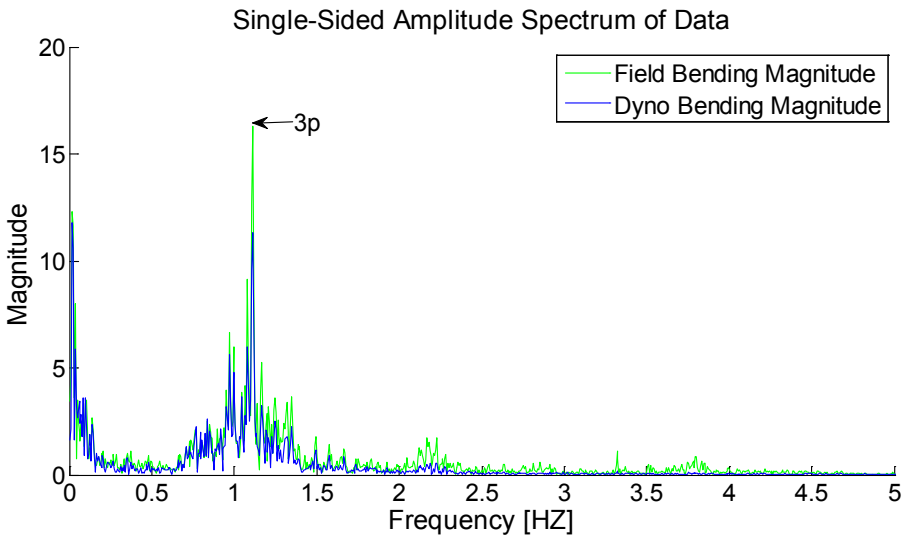

Figure 23. FFT of field shaft bending reproduced in dynamometer testing.

This new capability in dynamic non-torque loading allows the NREL 2.5-MW dynamometer to capture non-torque field loading conditions without the costs associated with in-field test operations. Further advancement and analysis of this tool will allow the GRC team to analyze the effect of other field and dynamometer variables, such as tower structural vibrations, while forcing the system with the equivalent rotor loads it will experience in the field.

5 Conclusions

Gearboxes designed for wind turbines do not always achieve the 20 year design life as required in the IEC 61400-1 standard (7). Commercial and intellectual property considerations have hindered the solution of the problems with the gear and bearing elements, but it is clear that something fundamental is missing in the overall process of specifying, designing and validating gearboxes for this unusual application. As part of an effort to address these shortcomings, the GRC is evaluating dynamometer test approaches that reproduce the loading conditions a gearbox will experience in the field.

Two identically rebuilt and instrumented gearboxes were tested on a nacelle in the NREL dynamometer and on a turbine in the field. In comparing GRC field and dynamometer test data, we have reached the following conclusions:

- Dynamic non-torque load testing is able to reproduce the bending moment variations measured in the field.
- The non-torque loads have an appreciable effect on ring gear face width load distribution. This illustrates the importance of accurately reproducing these loads in dynamometer testing.

- Torque variations in the field are not reproduced in typical dynamometer testing. These variations can be reproduced in the dynamometer but limitations in the test equipment must be considered because they can introduce unwanted dynamics. The lessons learned in our attempts to reproduce field torque time histories will be applied to the control of NREL's 5 MW dynamometer.
- The planets experience a 1p cyclical load share variation. Further modeling and analysis should reveal whether dynamic loads above 1p have a significant effect on the bearing load distribution.

The data sets will eventually become publicly available to those willing to share their analysis. Currently, the NREL GRC is working with our analysis partners to use test data to advance the state of the art of drivetrain design tools.

6 Future Plans

The knowledge that is gained by analyzing the first phases of testing and comparing that data to the modeling efforts will be used in the next phase of the GRC. This phase will consist of a review of the design process that was executed as part of the GRC for the first two test articles. In addition this next phase will consist of a redesign of one of the gearboxes to make small design changes. The redesign will allow for additional instrumentation in those areas where the modeling has shown the need for validation. An enhanced field test is also envisioned for the coming year.

7 Acknowledgments

The National Renewable Energy Laboratory's GRC work is funded by the Wind and Water Power Program, Office of Energy Efficiency and Renewable Energy of the U.S. Department of Energy under Contract No. DE-AC02-05CH11231. The authors would like to acknowledge the contributions of several individuals who have helped formulate the ideas and actions expressed in this paper including Sandy Butterfield, Walt Musial, Don McVittie, Bob Errichello, Ed Hahlbeck, Francisco Oyague, and Hal Link. In addition, the U.S. Department of Energy is recognized for its continued support of this project.

8 References

1. Musial, W. D., Butterfield, C. P. and McNiff, B. "Improving Wind Turbine Gearbox Reliability," Proceedings of EWEC 2007, Milan, Italy, April 2007.
2. Oyague, F., Gorman, D., and Sheng, S., "NREL Gearbox Reliability Collaborative Experiemental Data Overview and Analysis," NREL/CP-500-48232, May 2010.
3. Peeters, J., Vandepitte, D., and Sas, P., "Analysis of Internal Drivetrain Dynamics in a Wind Turbine," *Wind Energy*. DOI: 10.1002/we.173, John Wiley and Sons, July 2005.

4. *Windpower Monthly*, "Facing up to the Gearbox Challenge: A survey of gearbox failure and collected industry knowledge," Volume 21 (11), November 2005.
5. Rasmussen, F., Thomsen, K., and Larsen, T. J., "The Gearbox Problem Revisited*,"*Risø Fact Sheet AED-RB-17(EN), Risø National Laboratory, Roskilde, DK, 2004.
6. International Electrotechnical Commission. "Wind Turbines – Part 4: Standard for Design and Specification of Gearboxes," ISO/IEC 61400-4 DIS, ISO Geneva, Switzerland.
7. International Electrotechnical Commission. "Wind Turbine Generator Systems - Part 1: Safety Requirements," IEC 61400-1, Ed. 3. IEC, Geneva, 2004.
8. International Organization for Standardization: ISO 281:2010. "Rolling bearings - Dynamic load ratings and rating life," ISO Geneva CH, 2010.
9. McNiff, B, van Dam, J., et al. "Gearbox Reliability Collaborative: Phase 1 Test Plan," National Renewable Energy Laboratory, Draft Publication December 2009, to be published.
10. van Dam, J., "Gearbox Reliability Collaborative Bearing Calibration" ; NREL Report No. TP-500--47852.
11. Crowther, A. R., Ramakrishnan, V., Zaidi, N. A., and Halse, C. "Sources of time-varying contact stress and misalignment in wind turbine planetary sets," *Wind Energy*. DOI: 10.0069, John Wiley and Sons, 19 May 2010.
12. International Organization for Standardization: ISO 6336-1:2010 "Calculation of load capacity of spur and helical gears," ISO Geneva CH, 2010.
13. American Gear Manufacturers Association, ANSI/AGMA 6123-BXX, "Design Manual for Enclosed Epicyclic Gear Drives," AGMA, Virginia USA, 2006.

Appendix A: Coordinate System

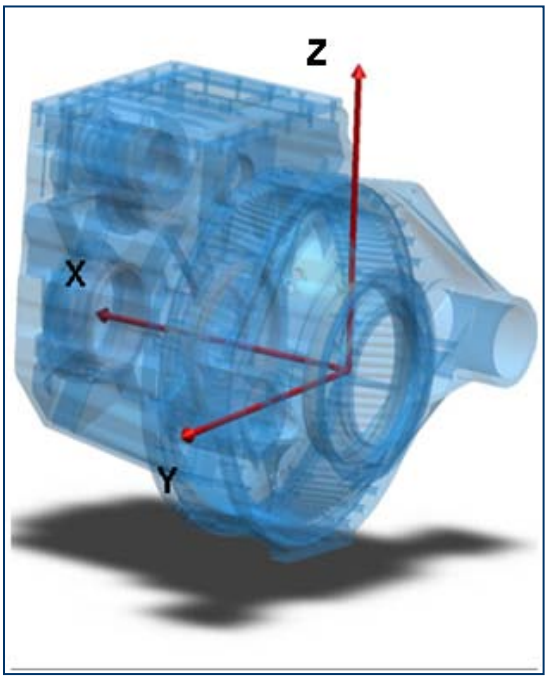

Figure 24. Coordinate system for gearbox and nacelle.

The coordinate system implemented in this document follows the IEC standard (6). It is a right hand coordinate system where the X axis is aligned with the drive shaft and therefore has a 5 degree tilt with respect to the inertial frame. The coordinates describing the orientation of the load or bending are polar coordinates with 0 degrees at top dead center of the main bearing. The angle increases in the clockwise direction while pointing down wind. Figure 24 and Figure 25 show a visual representation of the coordinate system used in this document.

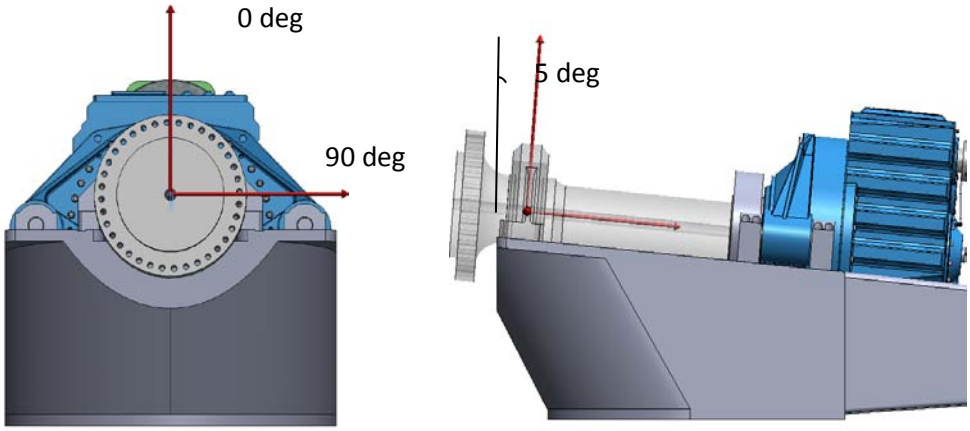

Figure 25. Main shaft moment orientation and reference.

In the case of the moments, the angle in Figure 25 describes the direction of the vector in which a positive moment is applied in accordance with the right hand rule. Figure 26 shows a moment with a direction of 90 degrees. With respect to the axes, this is a negative moment in the Y direction.

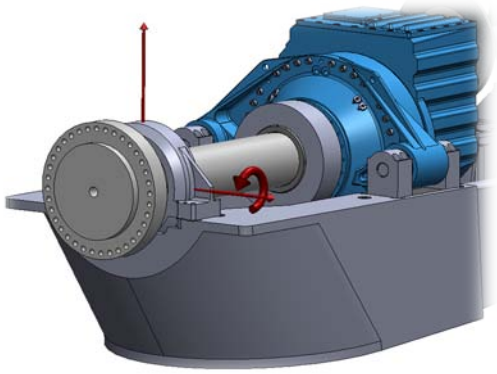

Figure 26. Negative gearbox pitch moment (-Y) reference.

Port refers to the negative Y direction and Starboard refers to the positive Y direction.